Stress Transfer Quantification in Gelatin-Matrix Natural Composites with Tunable Optical Properties

Franck Quero[1,], Abigail Coveney[2, 3], Anna E. Lewandowska[4], Robert Richardson[3], Paulo Díaz-Calderón[1], Koon-Yang Lee[5], Stephen J. Eichhorn[4], Ashraf Alam[3], Javier Enrione[1]*

1. Universidad de los Andes, Av. Monseñor Álvaro del Portillo 12.455, Las Condes, Santiago 7550000, Chile

2. Bristol Centre for Functional Nanomaterials, Centre for NSQI, University of Bristol, Tyndall Avenue, Bristol BS8 1FD, UK

3. H. H. Wills Physics Laboratory, University of Bristol, Tyndall Avenue, Bristol BS8 1TL, UK

4. College of Engineering, Mathematics & Physical Sciences, University of Exeter, Harrison Building, North Park Road, Exeter EX4 4QF, UK

5. The Composites Centre, Department of Aeronautics, Imperial College London, South Kensington Campus, London SW7 2AZ, UK

KEYWORDS Gelatin, bacterial cellulose, composites, optical properties, stress transfer.

ABSTRACT

This work reports the preparation and characterization of natural composite materials prepared from bacterial cellulose (BC) incorporated into a gelatin matrix. Composite morphology was studied using SEM and 2D Raman imaging revealing an inhomogeneous dispersion of BC within the gelatin matrix. The composite materials showed controllable degrees of transparency to visible light and opacity to UV light depending on BC weight fraction. By adding a 10 wt.% fraction of BC in gelatin, visible (λ = 550 nm) and UV (λ = 350 nm) transmittances were found to decrease by ~35 and 40 %, respectively. Additionally, stress transfer occurring between the gelatin and BC fibrils was quantified using Raman spectroscopy. This is the first report for a gelatin-matrix composite containing cellulose. As a function of strain, two distinct domains, both showing linear relationships, were observed for which an average initial shift rate with respect to strain of -0.63 ± 0.2 $cm^{-1}\%^{-1}$ was observed, followed by an average shift rate of -0.25 ± 0.03 $cm^{-1}\%^{-1}$. The average initial Raman band shift rate value corresponds to an average effective Young's modulus of 39 ± 13 GPa and 73 ± 25 GPa, respectively for either a 2D and 3D network of BC fibrils embedded in the gelatin matrix. As a function of stress, a linear relationship was observed with a Raman band shift rate of -27 ± 3 cm^{-1} GPa^{-1}. The potential use of these composite materials as a UV blocking food coating is discussed.

INTRODUCTION

Natural polymer materials have been the focus of considerable recent scientific and industrial attention due to some of their unique intrinsic properties. Such properties include their renewable origin, potential biodegradability, non-toxicity, human edibility, and indigestibility. A commonly

used biopolymer is gelatin, a protein-based natural polymer material. Gelatin is obtained from collagen, a fibrous protein and is typically extracted from the connective tissues including skin, tendon or ligaments of animals (mostly cattle, pork, fish and chicken). There are two types of gelatin; type A and type B that are derived from collagen using an acid-based or alkaline hydrolysis process, respectively.[1] Gelatin is currently used in the pharmaceutical, food, photography and cosmetic industries, most commonly as a gelling agent.[2,3] In addition to this, gelatin has demonstrated tremendous potential for other applications including tissue engineering[4,5] and food coatings.[6] Gelatin is, however, brittle (especially in its dried state) and moisture sensitive which implies that the physical properties of gelatin are highly dependent on humidity where gelatin is exposed to.[7] To overcome these limitations, the most commonly applied strategy is to chemically cross-link gelatin.[8]

An alternative approach to improve the physical properties of gelatin including mechanical properties and sorption properties has been to develop natural polymer based micro- and nanocomposite materials with other natural polymers as fillers. In particular, cellulose nanocomposites have recently attracted attention as materials with improved physical properties including mechanical, thermal and optical characteristics.[9] Also, adding micro- and nanoparticles to gelatin could enable the design of biopolymer-based materials with specific properties for a range of applications including encapsulations of drugs, food coating or scaffolds for tissue engineering. Over the past few years, a variety of nanocellulose-based composites have been reported[10], including microfibrillated cellulose (MFC)[11] (also referred to as nanofibrillated cellulose), bacterial cellulose (BC)[12] and cellulose nanocrystals.[13,14] Nevertheless, little information on the fundamental nature of the interaction between these filler materials and gelatin exists. In the gelatin-MFC[11] and gelatin-BC nanocrystal[13] studies, cellulose was found,

for example, to significantly reduce the water sorption capacity of gelatin, probably due to its relatively high crystallinity. The addition of BC nanocrystals was also found to significantly increase thermal and mechanical properties of gelatin.[13] A recent study, reported a decrease in tensile strength upon addition of MFC and cellulose nanocrystals to gelatin[15] but an improvement in the barrier properties with respect to oxygen permeation. None of these three studies, however, have evaluated the effects of the addition of cellulose on the formation of the triple helix configuration in gelatin. No study has quantified the UV-transparency of gelatin-cellulose materials, but only focused on visible-transparency. MFC was found to lead to a small but significantly reduction in visible-transparency of gelatin.[11] Similar conclusions were reached for nanocellulose/gelatin nanocomposites although this was not quantified and only visually observed.[15] Consequently, designing gelatin/cellulose composites showing both visible-transparency and UV-opacity are challenging and have technological interest.

Cellulose is the most abundant naturally occurring semi-crystalline polymer on earth.[16] Thus, cellulose is an ideal candidate to be used as a renewable, biodegradable and non-toxic filler in a natural polymer matrix to create all-natural polymer composite materials. The high elastic modulus associated with the crystalline regions of cellulose implies that they have potential to be used as effective nano-filler to reinforce a polymer matrix. Bacterial cellulose (BC) fibrils have attractive mechanical properties. Young's modulus of BC fibrils have been evaluated using a cantilever AFM method as well as Raman spectroscopy; values of 78 ±17 GPa[17] and 79-88 GPa[18] were obtained, respectively. This shows the potential of BC fibrils for reinforcing brittle natural polymer matrices such as gelatin. BC fibrils have been shown to be an efficient filler in various biocomposite systems. Successful improvement of Young's modulus of starch,[19] poly(lactic acid) (PLA)[20,21], cellulose acetate butyrate[22], green polyurethane[23] or fibrin[24] using

BC fibrils as filler has been demonstrated and a lot more examples have been reported in the literature.[10]

BC can be cultured under static conditions.[25] At the end of the static culture process, a pellicle containing a three-dimensional (3D) network of BC nanofibrils is obtained. After disintegration of the never-dried gelatinous pellicle, a water-soluble polymer can be added to obtain a nanocomposite material.[19] It is important to keep the system wet to avoid strong aggregation of BC fibrils into larger elements and eventually obtain a good dispersion in the surrounding polymer matrix. Strong aggregation of BC fibrils into larger elements is induced by the formation of hydrogen bonding. High transport costs and a risk of bacterial contamination associated with aqueous conditions, however, have resulted in significant interest in the development of a method to re-fibrillate cellulose from a dried source into individual cellulose fibrils.

This work presents a straightforward approach for the preparation and characterization of gelatin-BC composites from re-wetted BC pellicles. In addition, this study demonstrates that a degree of aggregation of BC fibrils, generating local inhomogeneities, can provide benefits to the composite materials such as the blocking of ultraviolet (UV) light while maintaining a good degree of visible transparency. Local inhomogeneties in cellulose-based composites are not untypical and have been reported before but in this work it is demonstrated that these local inhomogeneities can provide benefits for the use of gelatin-cellulose composites as food coatings or encapsulating agents. This work also demonstrates, for the first time, that it is possible to quantify stress transfer from gelatin to bacterial cellulose using Raman spectroscopy. The potential of these materials to be used as food coatings for fresh food preservation is discussed.

EXPERIMENTAL SECTION

Materials. Dried BC pellicles were kindly provided by Membracel® (Curitiba, Brazil). Bovine gelatin type B (Bloom 220) was purchased from Rousselot (Sao Paulo, Brazil) in a powder form. All chemicals were used as received without further purification. Silica gel was purchased from Winkler Ltd (Santiago, Chile).

Preparation of Gelatin-BC Composite Films. Firstly, 5 g of air-dried BC, in the form of tiny pieces of pellicles, was added to 1.2 L of de-ionized water (electrical conductivity ≤5 μS cm^{-1}) and allowed to soak overnight. The BC-water mixture was then blended using a standard kitchen blender (Thomas "Premium") for 20 minutes, followed by gravimetric filtration using filter paper (Whatman™ 541) to obtain a wet BC filter cake. In a separate experiment, a 7 w/v % aqueous gelatin solution was prepared by dissolving 10.5 g of bovine gelatin in 150 mL of water at 60 °C. The solution was stirred with a magnetic bar for 1 hour to allow for complete dissolution of the gelatin powder into deionized water. The previously prepared wet BC filter cake was then added to this gelatin solution and stirred again for 1 hour. The pH of the aqueous gelatin-BC suspension was adjusted by adding the necessary amount of sodium hydroxide and hydrochloric acid to reach a value of ~5. This corresponds to a zeta potential value of 2-3 mV.[26] Gelatin and gelatin-BC model composite films were then obtained by casting into the bottom part of polystyrene Petri dishes and subsequent drying at 5 °C for two weeks to allow for water evaporation. The films were then placed in a desiccator containing silica gels for at least a month to produce films with controlled moisture content. Moisture equilibrium was verified gravimetrically until constant weight was reached for all the materials with the exception of BC. The gelatin-BC gelatin composites were prepared with BC weight fractions of 0.5, 2, 6 and 10 wt.%.

Crystalline Structure of BC, Gelatin and Gelatin-BC Composites by XRD. X-ray diffraction (XRD) was used to obtain information on the crystallography of BC, gelatin and gelatin-BC composite films using an X-ray diffractometer (Phillips X'Pert Pro). The diffractometer was equipped with CuKα radiation source (1.541 Å) operated at a current and an accelerating voltage of 30 mA and 40 kV, respectively. The spectra were recorded from 2θ = 5 to 50 ° using a step size of 0.02 °. All measurements were performed in triplicated. The crystallinity index (*CI*) of BC pellicles was determined using Segal's method[27] and the equation:

$$CI = \frac{I_{002} - I_{\text{am}}}{I_{\text{am}}} \times 100 \quad (1)$$

where I_{002} and I_{am} correspond to the intensity of the 002 reflection plane and the intensity of the amorphous phase of cellulose (2θ = 18 ° for CuKα X-ray source). The diameter of the triple-helix of gelatin was obtained by calculating the *d*-spacing using Bragg's law[28], defined by the equation:

$$n\lambda = 2d\sin\theta \quad (2)$$

where *n* is the order of the reflection, λ is the wavelength of the X-ray source, *d* is the lattice spacing of the material's crystal structure (distance between atomic planes) and θ is the angle between the incident beam and the scattering planes.

For the XRD pattern of gelatin and gelatin-BC composite films, the area under the peak located at 2θ = 9 ° was determined by integration using the software package PeakFit v4.12

assuming a Lorentzian function fit. The peak integrals were then normalized with respect to the weight fraction of gelatin in the composite materials.

Thermal Properties of BC, Gelatin and Gelatin-BC Composites. A power compensation differential scanning calorimeter (Pyris 1 DSC, Perkin Elmer) was used to obtain the thermal properties of the samples. The calorimeter was calibrated using an indium standard ($T_{melting\ onset}$= 156.6 °C, ΔH_m = 28.5 J g^{-1}). An empty pan was used as reference. Approximately 15 mg of sample were hermetically sealed in 30 μL stainless steel pans. The samples were first cooled to -30 °C at a rate of 30 °C min^{-1} and maintained for 5 min prior to be heated to 190 °C at a rate of 10 °C min^{-1}. These experiments were performed in order to directly relate the film formation process to the enthalpy of melting of gelatin and gelatin-BC composites. The enthalpy of melting of the gelatin in the composites (ΔH_{m1}) was calculated using the equation:

$$\Delta H_{m1} = \left(\frac{\Delta H_{m2}}{f_c} \right) \quad (3)$$

where ΔH_{m2} is the measured enthalpy of melting of the samples determined from DSC and f_c is the weight fraction of gelatin in the sample (i.e. 1, 0.99, 0.98, 0.94 and 0.90). All measurements were triplicated.

Thermogravimetric analysis (TGA) was carried out using TGA Q500 (TA Instruments). Sample mass of 5 - 10 mg were heated in a platinum crucible from room temperature to 700 °C at a rate of 10 °C min^{-1} in N_2 atmosphere, with a N_2 flow rate of 40 mL min^{-1}. All measurements were triplicated. Onset and peak degradation temperatures were determined from the first derivative of the weight as a function of temperature using the software Universal Analysis 2000.

Density of Gelatin and Gelatin-BC Composites. Helium pycnometery (Accupyc 1330, Micromeritrics) was used to determine the density of gelatin and gelatin-BC composites. The samples were weighed prior to placing them in the measuring chamber of the helium pycnometer. As the pressure of helium rises above atmospheric pressure, it was expanded through a valve and this expanded volume was measured. Due to the expansion of helium, the pressure inside the measuring chamber will drop to a steady-state value. The density of the samples (ρ_m) were then calculated using the equation:

$$\rho_m = \frac{m_s}{V_c - \frac{V_E}{\left(\frac{P_1}{P_2} - 1\right)}} \quad (4)$$

where m_s, V_c, V_E, P_1 and P_2 are the mass of samples, measuring chamber's volume, expanded volume, chamber's elevated pressure and steady-state pressure, respectively.

Morphology of Gelatin and Gelatin-BC Composites. Scanning electron microscopy (SEM) (EVO MA 10, Carl Zeiss, Germany) was used to observe cryofracture surfaces of gelatin and gelatin-BC composites. An acceleration voltage of 25 kV was used. Prior to SEM, the samples were gold coated using a diode magnetron sputtering coater (model 12161, USA) and fixed onto metal stubs using carbon tabs.

The surface and sub-surface morphology of gelatin and gelatin-BC composites was studied by 2D Raman microscopy (XploRA^{TM} PLUS) equipped with a near infrared (785 nm) laser having a diameter of ~1 μm, a diffraction grating with groove density of 600 g mm^{-1} and an optical microscope (Olympus BX41) with a 50× long-working distance objective (PL Fluotar, NA=

0.55). The maximum penetration depth associated with 785 nm wavelength laser is ~12 μm. The laser power at the sample surface was kept at 70 mW, which was found not to induce sample burning. Each image was obtained by collecting 35 Raman point spectra, with an image quality sufficient to obtain information mainly from the surface distribution of BC embedded in the gelatin matrix. The spatial resolution used to obtain images was ~1 μm. Raman spectra were acquired using an exposure time of 10 s with 10 accumulations and normalized to the range of the cellulose band located at ~1095 cm^{-1}.[29] Baseline correction was also applied to each of the collected Raman spectrum. Each image corresponds to a sample area of 0.01 mm^2.

In order to obtain 2D images from the surface and sub-surface of the gelatin-BC composites, a multivariate classic least square (CLS) fitting procedure was performed. This method can be used for multidimensional spectral arrays, including the generation of 2D images. For gelatin-BC composite materials, two reference spectra were used; one for the gelatin and one for the bacterial cellulose. This method allows the calculation of the contribution of each reference spectra within a mixed component spectrum (spectrum obtained for a composite material). The distribution of each reference component within a spectral array allows the creation of a 2D image based on the component distribution. The multivariate CLS analysis was implemented using LabSpec 6 software version 6.3. For example, this method has been also used to obtain 2D images of a model pharmaceutical Tablet, which contains microcrystalline cellulose.[30]

Optical Properties by UV-Visible Spectrophotometry. A Hitachi UV-visible spectrophotometer was used to measure the transparency of the composite films. Measurements were performed over the wavelength range of 200-1000 nm and data points were obtained with wavelength intervals of 50 nm. Gelatin and gelatin-BC composite films were placed perpendicular to the laser beam. Each measurement was performed subsequent to a calibration

reading corresponding to an empty transmittance accessory. Areas of the films having no significant difference in thickness were selected to carry out the measurements. These areas had a thickness of 0.16 ± 0.01 mm.

Stress Transfer Quantification in gelatin-BC composites using Raman Spectroscopy. Stress transfer from gelatin to BC was quantified using Raman spectroscopy. The measurements were performed using a Renishaw RM-1000 system equipped with a thermoelectrically cooled CCD detector. The laser was focused onto the samples using a Leica microscope with a ×50 objective lens. A 785 nm wavelength laser operating at maximum power was used to collect Raman spectra (1 mW power on the sample surface). The 10 wt.% BC sample was found to be the only composition in which the relevant band located at ~1095 cm^{-1}, corresponding to C-O and C-O-C stretching vibrations in the cellulose backbone, had sufficient intensity to determine its peak position accurately. The Raman spectrum of gelatin was also recorded to verify that gelatin and BC are spectroscopically distinct in the region of interest (1050 – 1150 cm^{-1}).

To study the micromechanics of the samples, specimens of gelatin-BC film with 10 wt.% BC were inserted into an *in situ* tensile and compression stage (Deben Microtest, 200N load cell). The samples (having thicknesses of 0.1 ± 0.01 mm, 10 mm widths and lengths of 20 – 30 mm) were deformed using extension steps of 0.02 mm with a motor speed of 1 mm min^{-1}. Raman spectra were recorded using a single accumulation at each strain increment with an exposure time of 120 s. Raman spectra were individually fitted using a Lorentzian function and an algorithm based on the work of Marquardt[31] in order to determine the position of the Raman band initially located at ~1095 cm^{-1} obtained at each tensile deformation increment. All measurements were carried out in triplicate. Average and standard deviation data are presented.

Young's modulus of the gelatin-BC composite ($E_{composite}$) containing 10 wt.% BC was estimated using the equation:

$$E_{composite} = \frac{d(\Delta\nu)}{d\varepsilon} \times \frac{d\sigma}{d(\Delta\nu)} \quad (4)$$

where $\Delta\nu$ is the Raman shift, ε and σ are the tensile strain and stress, respectively. A value of -4.3 cm^{-1} GPa^{-1} was used for $d(\Delta\nu)/d\sigma$ which corresponds to a calibration value obtained from a range of natural cellulose fibres[32] and has previously been used to calculate the effective Young's modulus of MFC and bacterial cellulose fibrils[18], and nanowhiskers embedded in polymeric resins.[33,34] The effective Young's modulus of a single BC fibril, embedded in gelatin, was calculated using Krenchel's relationship[35]:

$$E_{composite} = \eta_0 E_{fibril} \quad (5)$$

where E_{fibril} is the effective Young's modulus of a single BC fibril and η_0 is an efficiency factor equal to 3/8 for a 2D in-plane random network of fibrils and 1/5 for a 3D network of fibrils.

RESULTS AND DISCUSSION

XRD pattern of BC, Gelatin and Gelatin-BC Composites. Figure S1 (Supporting Information) shows a typical XRD pattern of BC. The diffraction peaks observed for BC are characteristic of a cellulose I polymorph,[36,37] with typical diffraction planes of (101), ($10\bar{1}$), (002) and (040). The crystallinity index of the BC prior to blending was found to be 94.5 ± 0.5

%. Nevertheless, it should be noted that the crystallinity index calculated from the Segal's equation is generally considered to overestimate crystallinity of cellulose.[38,39] The XRD diffraction pattern of gelatin is reported in Figure 1. A broad background with a peak intensity located at ~21° is observed and is typical of the amorphous fraction of gelatin and collagen.[40] The peak located at $2\theta = 9°$ corresponds to the triple helix structure present in collagen and renatured gelatin[11,40] and the intensity of this peak has been shown to be proportional to the triple helix content (THC) of gelatin based materials.[7,40,41] The triple helix diameter was estimated using Bragg's law[28], and found to be 0.99 ± 0.02 nm. This value is similar to those previously reported using XRD[40] and AFM imaging.[26]

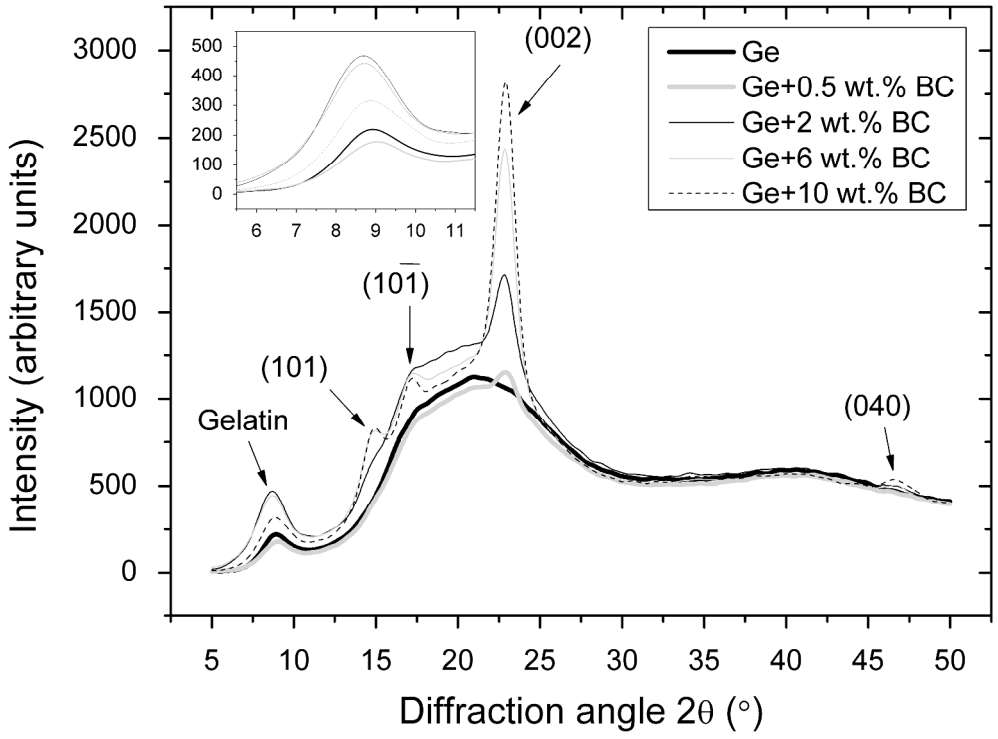

Figure 1. Typical X-ray diffraction patterns for gelatin and gelatin-bacterial cellulose (BC) composites at various weight fractions (wt.%). The inset represent the diffraction peak located at approximately 2θ = 9°, corresponding to the triple helix configuration of gelatin.

The XRD patterns of gelatin-BC composites are also shown in Figure 1. Diffraction peaks belonging to both the component materials can be identified, with the intensity of the cellulose peaks showing strong dependence on its content. For example, the diffraction pattern belonging to the 10 wt.% BC sample is almost entirely dominated by the cellulose peaks in the 2q range of 12 - 35°, whereas for the 0.5 wt.% sample they are barely visible and the hump located at ~21° corresponding to the amorphous fraction of gelatin is prominent. The presence of cellulose peaks superimposed with the XRD background corresponding to amorphous gelatin (12 - 35°) meant

that the area of this peak could not be accurately determined in order to quantify THC. Instead, the normalized integrals (proportional to the THC) of the triple-helix peak at $2\theta = 9\ ^\circ$ (Table 1) were analyzed and normalized with respect to the gelatin weight fractions. No significant trend in the normalized integrated peak was identified, as reported in Table 1. This suggests that the presence of BC does not induce additional triple-helix formation in the gelatin matrix. This observation is commensurate with the enthalpy of melting obtained from DSC, as displayed in Table 1, which also does not show a significant change in the proportion of the enthalpy of melting (also proportional to the THC) of gelatin across the composition series.

Table 1. Normalized integrated area for the peak located at 2θ = 9 ° in the gelatin phase for BC composite films as measured using XRD, enthalpy of melting obtained from DSC and density from gas pycnometry experiments

Bacterial cellulose content (wt.%)	Normalized integrated peak area at 2θ = 9 ° (arbitrary units / °)	Enthalpy of melting, ΔH_m (J g^{-1})	Density (g cm^{-3})
0	4 ± 2	18 ± 1	1.505 ± 0.001
0.5	5 ± 2	18 ± 2	1.503 ± 0.001
2	7 ± 1	18 ± 0	1.504 ± 0.001
6	6 ± 1	17 ± 0	1.515 ± 0.001
10	3 ± 3	16 ± 1	1.519 ± 0.003

Thermal Degradation Behavior of BC, Gelatin and Gelatin-BC Composites. Figure 2 reports typical TGA curves for BC, gelatin and gelatin-BC composites. There is evidence of weight loss due to evaporation of moisture starting at approximately 100 °C, followed by thermal degradation starting at approximately 250 °C. Comparison of percentage weight loss at 500 °C shows no significant deviation across the composition range of the composite materials. The onset and peak degradation temperatures of the composites are seen to significantly increase with BC content as reported in Table S1 (Supporting Information) and as shown in the inset in Figure 2. This suggests that BC acts to improve the thermal stability of the composite materials. Moreover, the properties of the BC component have been fully realized. This is supported by the

prediction of the peak degradation temperature using the rule of mixtures as reported in Table S1. At a BC weight fraction of 10 wt.%, the experimental value for the peak degradation temperature is even higher than the prediction from the rule of mixtures. This may be due to a high level of gelatin/BC and inter-BC fibril hydrogen bonding interactions, which could thermically stabilizes the gelatin-BC 10 wt.% composite materials. An understanding of the thermal behavior of the composite materials is key, as it will have implications for energy intensive processing including spray-drying, extrusion.

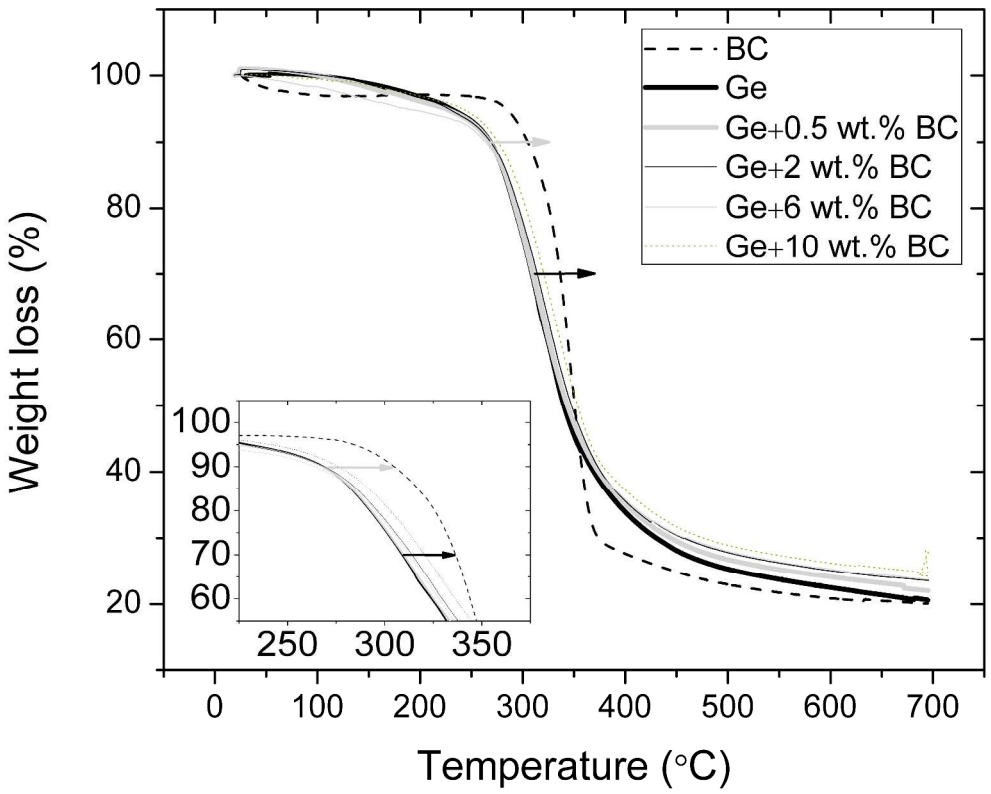

Figure 2. Typical thermograms for BC, gelatin and gelatin-BC composites. The arrows give an indication of the shift of the onset (grey) and peak (black) degradation temperatures towards a higher temperature upon addition of BC to the gelatin matrix. The inset represents the same thermograms from 225 to 375 °C.

Density of Gelatin and Gelatin-BC Composites. As the component materials of the composite have similar bulk densities, as reported in Table 1, variation in the density across the composition range would not necessarily be expected because gelatin and BC have similar densities of ~1.5 g cm^{-3}. It is, however, possible that voids could be formed at the interfaces between the matrix and the BC inclusions or introduced as part of the preparation and film

formation process. Gas pycnometry experiments show no significant change in density as a function of BC content as shown in Table 1, indicating that no porosities were introduced during the film fabrication and formation process. This preservation of density is an important advantage, as additional porosity is likely to reduce the barrier properties of the material, reducing its suitability for encapsulation/food coating applications. Porosities or voids may also induce visible light scattering and so reduce transparency.

Morphological Analysis of Gelatin and BC-Gelatin Composites. Figure 3 reports images from the cryofracture surfaces of gelatin and gelatin-BC composites (2 and 6 wt.%). A layered structure along the depth of the samples can be observed for gelatin and gelatin-BC composites. Images of the composite materials indicate that this layered structure is maintained with BC fibrils and BC present in-between gelatin layers. The presence of BC fibril agglomerates is clearly observed in the composite samples, as shown by the black arrows in Figures 3b and 3c.

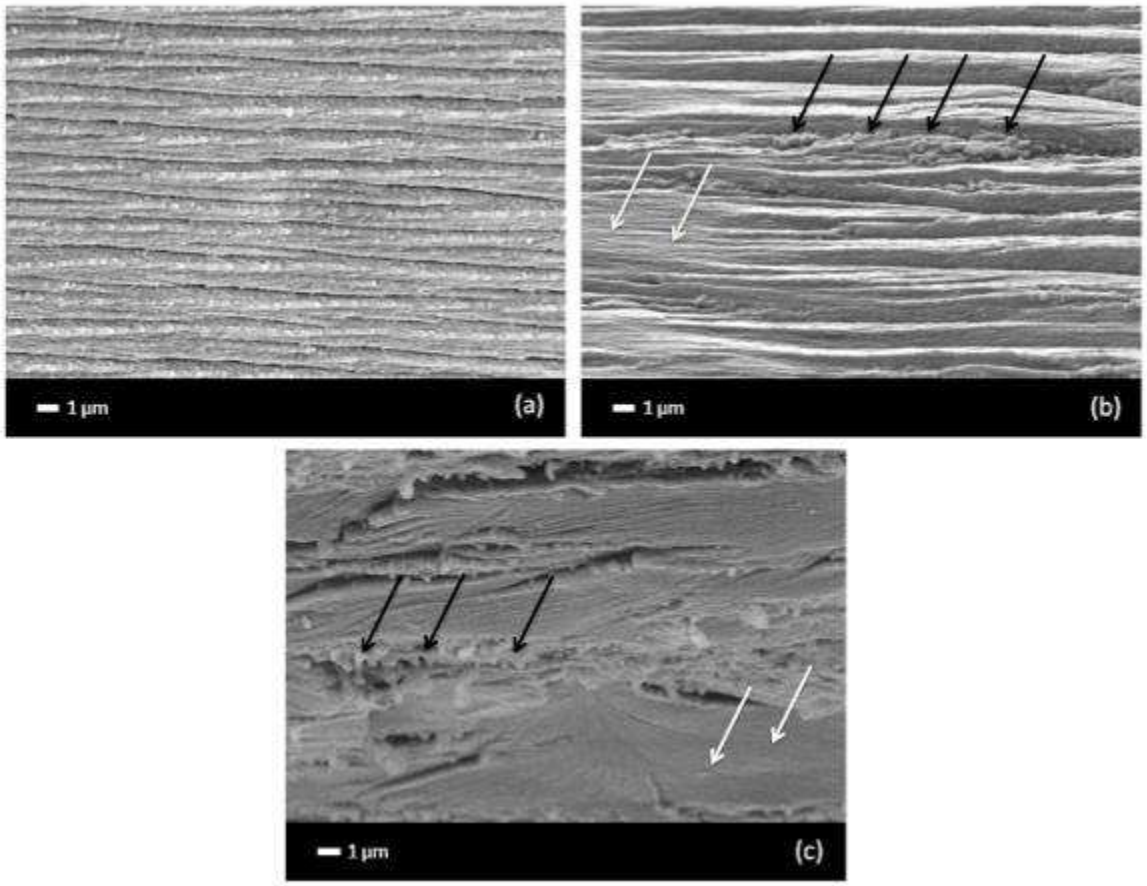

Figure 3. Scanning electron microscopy images of the cross-section of gelatin (a) and gelatin-bacterial cellulose composites with compositions 2 wt.% (b) and 10 wt.% (c). Black and white arrows show respectively BC fibrils and gelatin.

2D Raman mapping images was carried out to study BC distribution across a large size range. It is important to mention that the Raman band located at ~1095 cm-^{1}, arising from the presence of BC was the only one detectable in gelatin, which dominated the Raman signal generated by the composite materials. Regions where BC was not detectable were attributed to the presence of gelatin rich zones although BC might be present but was not detectable. Maps of the intensities of the Raman band from BC located at ~1095 cm^{-1} obtained from composites with BC loadings

0.5, 2, 6 and 10 wt.%, respectively are shown in Figure 4. An inhomogeneous distribution of BC can be clearly observed across all loadings. From 0.5 to 6 wt.% BC in gelatin matrix, an increase in BC concentration is observed represented by larger red areas. At a weight fraction of 10 wt.%, this trend is not followed. The image might represent a sparser region of the film surface, which might be a further indication of the inhomogeneous distribution of BC fibrils in the gelatin matrix at the surface and to a certain extent the sub-surface (up to ~12 μm). This information can, however, not be used to qualify the whole 3D structure. It is also possible that at a weight fraction of 10 wt.%, BC fibrils are more likely to form 'flocs' or agglomerates and so the gelatin and BC would partially phase separate during the film formation process. We, however, do not have direct evidence of this.

It is also important to consider in these images the possibility of slight overestimation of aggregation of BC. In these pictures, additive transmission from cellulose fibres may be observed since the NIR laser has a wavelength of 785 nm can slightly penetrate into the transparent gelatin matrix, thereby detecting cellulose fibrils located beneath the surface.

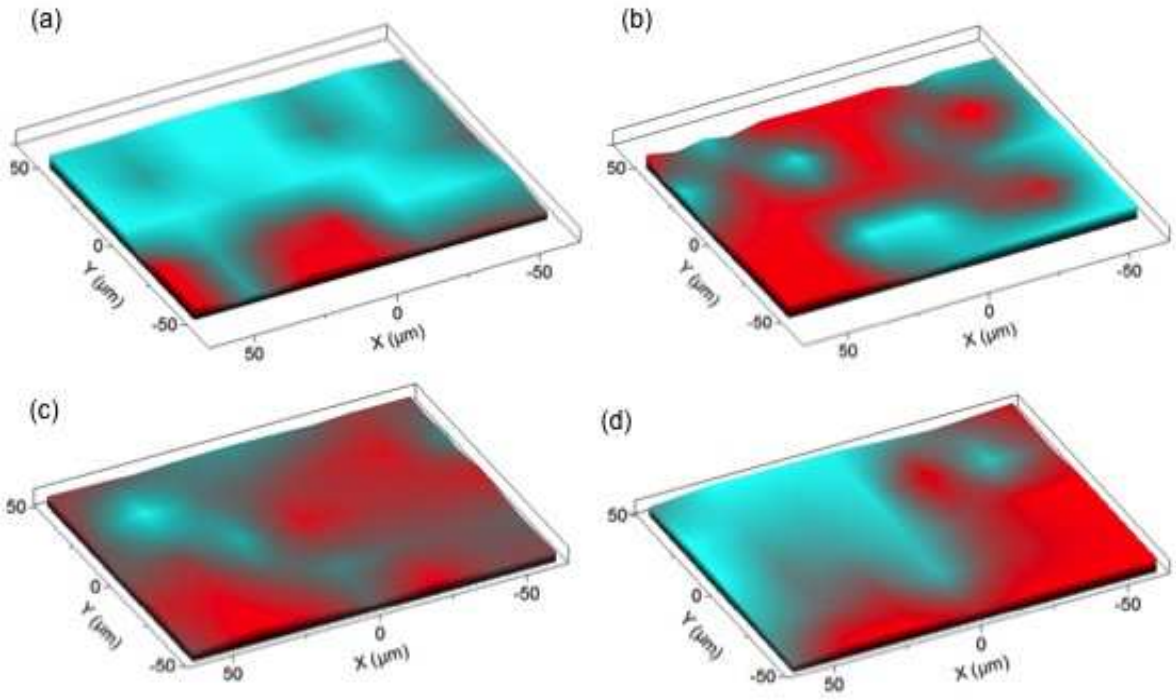

Figure 4. Typical 2D Raman images obtained from the surface of gelatin-BC composite films with compositions: 0.5 wt.% (a), 2 wt.% (b), 6 wt.% (c) and 10 wt.% (d). The red and blue colours are respectively assigned to the distributions of BC fibrils and the gelatin matrix. Grey regions represent the interface between gelatin and BC.

Optical Properties of Gelatin and Gelatin-BC Composites. The optical properties of gelatin and gelatin-BC composites were studied to assess their suitability to be used as transparent coating materials. Such a coating should maintain the aesthetic properties of the food or other product to be preserved *i.e.* where the transmittance of visible wavelengths should be optimized.

Figure 5 reports contact transparency images of gelatin and the composite materials. Contact transparency images are usually studied to assess the visual impact of the films. These contact transparency images suggest good optical visible transparency although some "cloudiness" is

observed for the composite materials having BC weight fractions of 6 and 10 wt.%, suggesting inhomogeneities. These "cloudy" regions however still retain sufficient degree of visible transparency. These translucent regions at the higher filler loadings (6 and 10 wt.%) can be attributed to large BC aggregates.

Figure 5. Image showing contact transparency of gelatin (a) and gelatin-bacterial cellulose composite films with BC loadings: 0.5 wt.% (b), 2 wt.% (c), 6 wt.% (d) and 10 wt.% (e). Scale bar corresponds to 1 cm. The logo is used with permission from Universidad de los Andes.

Figure 6 reports UV-Visible transmittance spectra of gelatin and gelatin-BC composites. The spectra show that the transmittance of visible light decreases from a range of 77.5 – 89.9 % for gelatin to a range of 46.8 – 60.8 % for the highest BC loading. This reduction can be attributed to light scattering by the BC fibrils aggregates and so to a relatively poor dispersion as suggested 2D Raman imaging. Surface roughness effect may also contribute to light scattering although we do not have direct evidence of this. The dimensions of BC filler may exceed the wavelength of visible light of 400 - 700 nm below which a composite is expected to be transparent, according to

Rayleigh's law.[42] One can also attribute the relatively good transparency of the composite materials to the fact that gelatin and cellulose have close refraction index and so the resulting composite will show transparency.[43] Cellulose and gelatin have respectively 1.618 (along the fiber) - 1.544 (transverse direction)[44] at a wavelength of 587.6 nm and 1.520 - 1.530[45] and 1.54 at a wavelength of 546.1 nm.[46]

A similar decrease in transmittance is observed for wavelengths in the UV region. The transmittance was found to decrease from 65 to 35 % at a wavelength of 350 nm for gelatin-BC composites containing 10 wt.% BC. This is, however, a beneficial property if these composite materials are to be used for UV-sensitive food coating applications[47,48] with the potential to prevent UV degradation of the coated food product while being, for example, displayed and stored under a supermarket's lighting system. This shows that BC aggregates present features favouring UV-opacity to the composite materials. This property is of importance for any UV-sensitive food products and other pharmaceutical or cosmetic compounds.

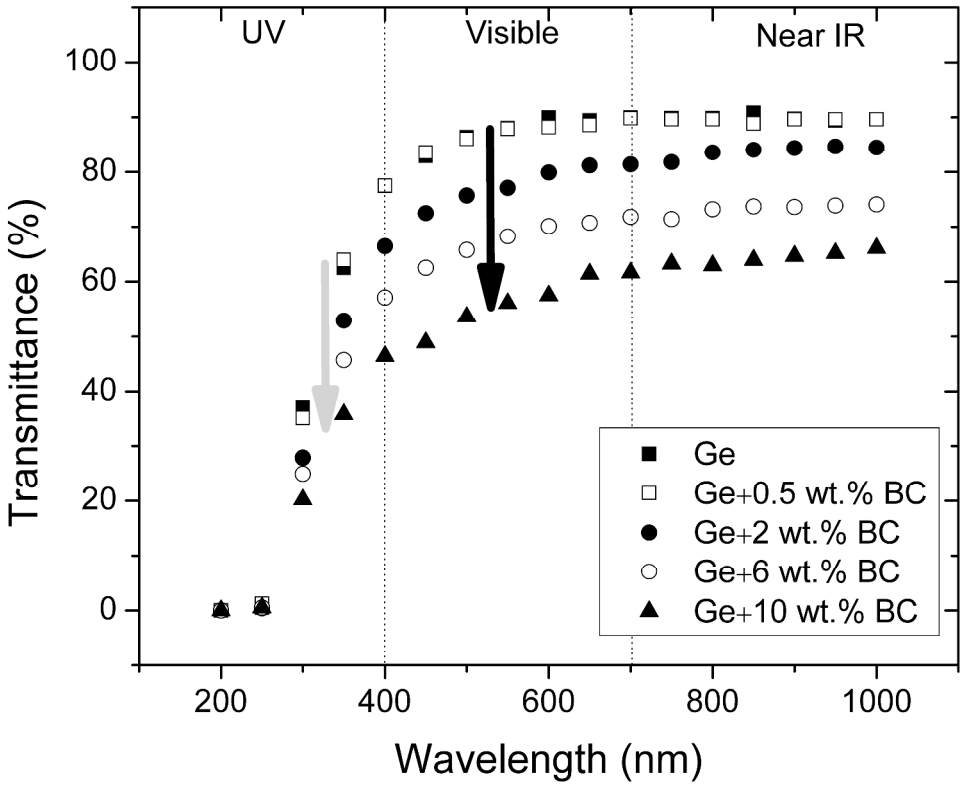

Figure 6. Transmittance spectra of gelatin (Ge) and Ge-bacterial cellulose (BC) composites with BC loadings 0.5, 2, 6 and 10 wt.%. The black and grey arrows indicate a reduction in transparency to visible and UV wavelengths, respectively.

Stress Transfer Quantification by Raman Spectroscopy. Figure 7 reports the Raman spectra of gelatin and gelatin-BC composites across the Raman shift range of 1050 – 1150 cm^{-1}. The Raman band located at ~1095 cm^{-1} seen in the composite samples is characteristic of cellulose and has been attributed to vibrational modes of C-O and C-O-C moieties.[29,49] As these bonds are present in the backbone structure of cellulose, the shift in the position of this band can be used to quantify stress in the cellulose fibrils.[32] This technique has been widely used to

understand mechanical reinforcement in cellulose fiber-based composites[50,21,33,34,51,52,53] but never in a gelatin-matrix composite. Since this Raman band from cellulose is spectroscopically distinct from any bands observed for gelatin, straightforward fitting of the cellulose peak is possible. In our range of compositions, only the 10 wt.% BC content offered sufficient intensity of the Raman band for an accurate determination of a shift in the peak position. For this reason, this was the only composition for which quantitative stress transfer evaluation was carried out.

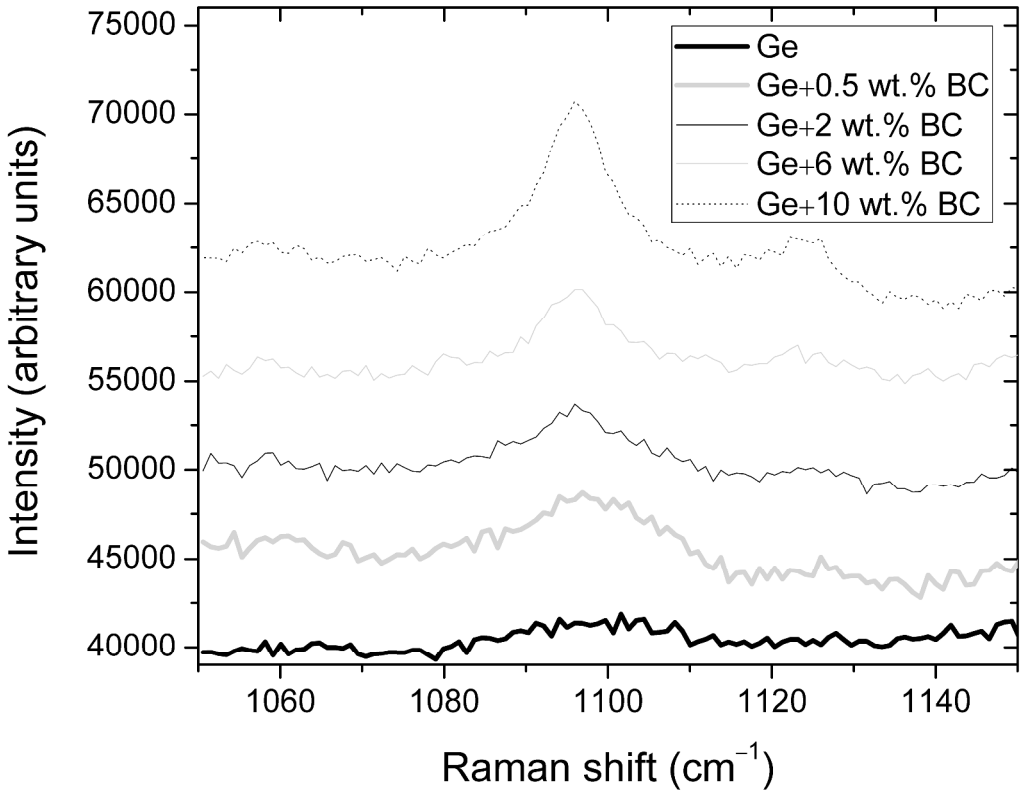

Figure 7. Typical Raman spectra for gelatin and gelatin-BC composite films (0.5, 2, 6 and 10 wt.%) in the Raman shift range of 1050 to 1150 cm^{-1}.

In Figure 8, a typical shift in the peak position towards a lower wavenumber of the Raman band initially located at ~1095 cm^{-1} at 0 and 5% strain is reported. This Raman band can be seen to significantly shift to a lower wavenumber position with increasing strain, confirming stress transfer from the gelatin matrix to the BC filler.

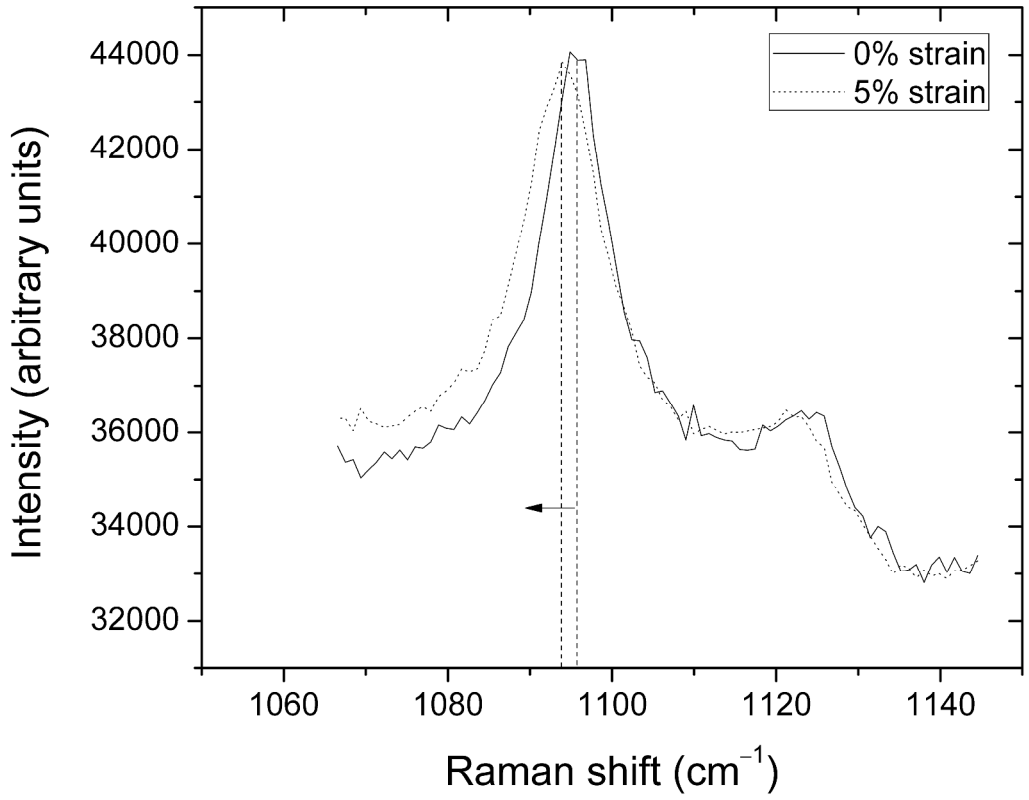

Figure 8. Typical shift towards a lower wavenumber position of the Raman band corresponding to vibrational modes of C-O and C-O-C moieties in the cellulose backbone upon application of external tensile deformation. Arrow indicates the direction of the band shift towards a lower wavenumber with increasing strain. Data are shown for a 10 wt.% gelatin-BC composite film.

A typical plot of Raman band shift as a function of strain is shown in Figure 9. Two distinct regions with average shift rates with respect to strain (found from linear fits to the data) of -0.73 $cm^{-1}\%^{-1}$ and -0.27 $cm^{-1}\%^{-1}$ are reported, which could be related to the transition from elastic to plastic deformation, respectively. Average shift rates of -0.63 ± 0.20 $cm^{-1}\%^{-1}$ and -0.25 ± 0.03 $cm^{-1}\%^{-1}$ were obtained from the average of three repeat experiments.

This change of Raman band shift rate was found to occur at a tensile deformation of approximately 1.5 %. The inset in Figure 9 is a typical stress-strain curve obtained while applying tensile deformation to the sample during the Raman spectroscopy experiments. Average Young's modulus, stress and strain at failure were found to be respectively 2.7 ± 0.6 GPa, 91.9 ± 4.2 MPa and 8.1 ± 0.7 % for 10 wt.% gelatin-BC composite films. Both linear and non-linear regions of the sample are identifiable from this curve. This change in mechanical response is observed at a strain of ~1 %; in close agreement with a change in Raman band shift rate possibly due to partial or interfacial decoupling between BC fibrils and gelatin, occurring close to the yield point. Similar interfacial rupture behavior characterized by a sudden change in the Raman band shift rate at a specific strain have been also identified previously for cellulose-containing composite materials.[21,53,18]

The average effective Young's modulus of BC fibrils embedded in gelatin was calculated using equations 4 and 5 and the average initial shift rate of -0.63 ± 0.20 $cm^{-1}\%^{-1}$ (possibly corresponding to the elastic deformation region), giving values of 39 ± 13 GPa and 73 ± 25 GPa assuming the BC fibrils as being present in either a 2D (η_0 = 3/8) or 3D (η_0 = 1/5) network, respectively. Although SEM imaging suggests a 2D in-plane orientation of BC fibrils, in reality the structure is likely to fall somewhere between this and a random 3D orientation. Therefore, it

is more likely that the actual effective Young's modulus value of BC in gelatin lies within the range of 39-73 GPa.

Recent work studying PVA/MFC[53] composites with a loading of 4 wt.% MFC reported a shift rate of -0.44 ± 0.06 $cm^{-1}\%^{-1}$, while a similar study of PLA/MFC composite materials[52] with 20 wt.% loading reported a shift rate of -0.38 ± 0.02 $cm^{-1}\%^{-1}$. In both cases, the Raman band shift rate was significantly lower than that found in our study here, indicating relatively more efficient stress transfer from the gelatin matrix to BC. This difference can be attributed to the superior intrinsic stress transfer efficiency observed in BC in comparison with MFC and to improved compatibility between filler and matrix associated with the use of hydrophilic gelatin in the place of hydrophobic PLA. Another contribution may originate from hydrogen bonding formation between gelatin and BC but also between BC fibrils themselves. We, however, do not have direct evidence in this work. Other studies have shown that higher Raman band shift rates can be obtained when BC is embedded in a PLA matrix, forming laminated composites. Raman band shift rates between -0.6 $cm^{-1}\%^{-1}$ and -2.0 $cm^{-1}\%^{-1}$ can be obtained depending on the culturing time or chemical modifications of the BC networks used to form the laminated composite materials.

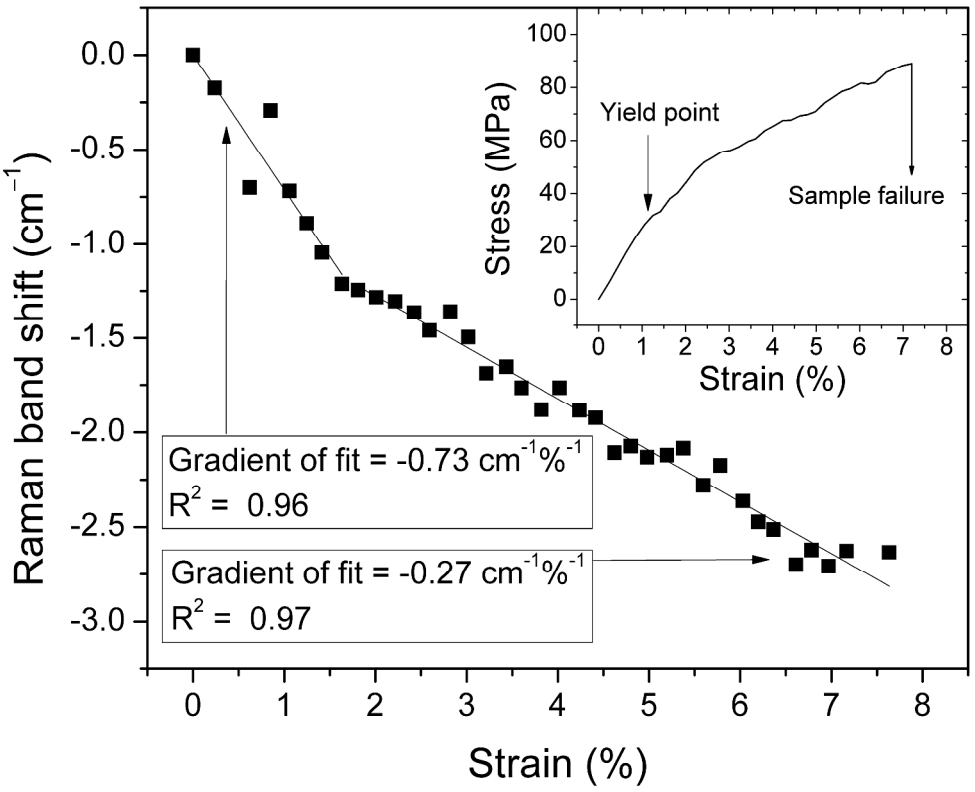

Figure 9. Typical shifts in the position of the Raman band corresponding to vibrational modes of C-O and C-O-C moieties in the backbone of cellulose as a function of strain. Results are shown for a 10 wt.% gelatin-BC composite film. The inset represents a typical stress-strain curve obtained for the same material. Solid lines are linear fits to the data.

Figure 10 reports typical detailed Raman band shifts as a function of stress for a 10 wt.% gelatin-BC composite film. Contrary to the data reported in Figure 8, the relationship between Raman shifts and stress is linear over the whole stress range. An average Raman band shift rate of -27 ± 3 cm^{-1} GPa^{-1} was found to occur, as a function of stress for the material containing 10

wt.% BC equivalent to a volume fraction of ~7 vol.% with the density of BC being 1.5 g cm^{-3}. This corresponds to a Raman band shift rate of -3.9 ± 0.4 cm^{-1} GPa^{-1} $vol.\%^{-1}$. This value is slightly higher than a value of -2.5 cm^{-1} GPa^{-1} $vol.\%^{-1}$ reported for poly(lactic acid) reinforced with bacterial cellulose networks[21], again probably due to enhanced hydrogen bonding between gelatin and inter-BC fibril hydrogen bonding interactions. The shift rate, if it could be accurately measurable by Raman spectroscopy at lower BC concentrations, would be expected to decrease at lower BC concentrations. This has been demonstrated for TEMPO-oxidized fibrillated cellulose composites, as a function of stress.[54]

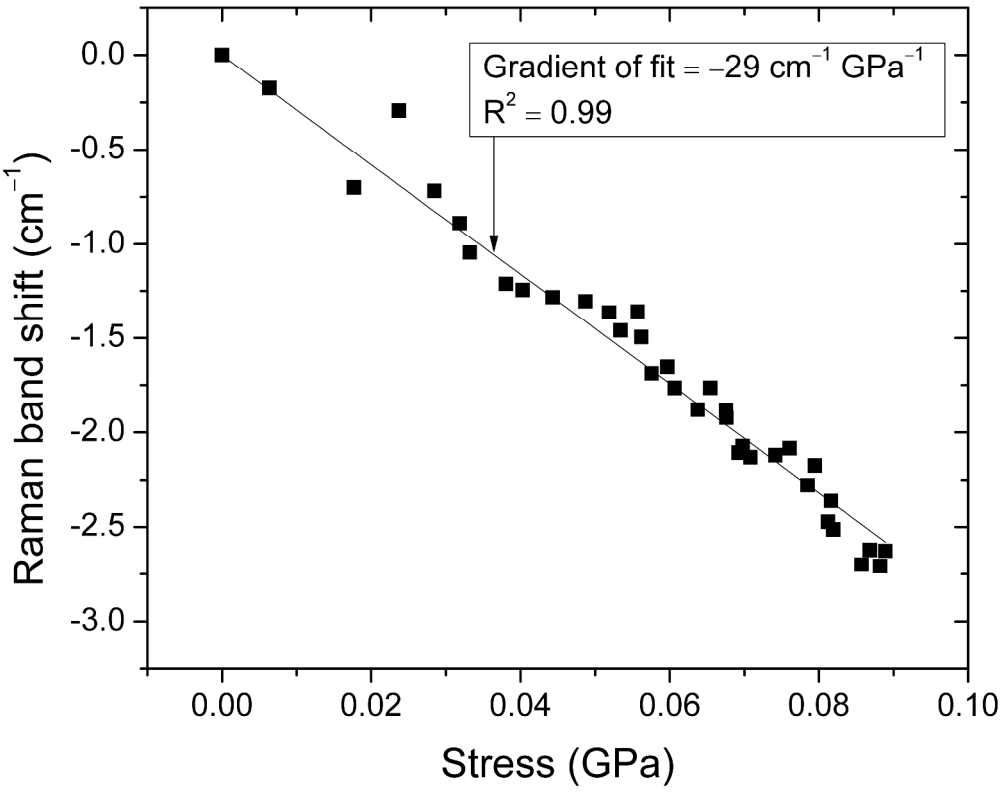

Figure 10. Typical shifts in the position of the Raman band corresponding to vibrational modes of C-O and C-O-C moieties in the backbone of cellulose as a function of stress. Results shown are for a 10 wt.% gelatin-BC composite film.

CONCLUSIONS

Natural composite materials have been prepared from re-wetted bacterial cellulose incorporated in a gelatin matrix. Results presented here suggest that these composite films have potential for food coatings and encapsulation applications owing to their tuneable optical properties and good stress transfer ability. Large aggregates of bacterial cellulose were observed,

which have been attributed to the strong inter-fibril interactions formed during its drying process (before re-fibrillation). By improving the disintegration technique and thereby increasing the interfacial area within the composite material, it is expected that stress transfer from the gelatin matrix to the fibers could be further enhanced. Despite the aggregation of fibrils, the films remain optically transparent, and yet also reduce transmittance of UV light. This work has also shown, for the first time, stress transfer processes occurring between gelatin and cellulose. Better stress-transfer is found for this system than other biopolymer-cellulose nanofiber combinations, which is encouraging for the development of mechanically robust, edible and sustainable coatings for foodstuffs.

ASSOCIATED CONTENT

Supporting Information. Typical XRD pattern for bacterial cellulose and detailed thermal degradation properties obtained by thermogravimetric analysis for gelatin, gelatin-BC composites and BC. This material is available free of charge via the Internet at http://pubs.acs.org.

AUTHOR INFORMATION

Corresponding Author

*E-mail: fquero@uandes.cl; Tel: (56-2) 2618 1108

Author Contributions

The manuscript was written through contributions of all authors. All authors have given approval to the final version of the manuscript.

Funding Sources

This research has been financially supported by el Fondo Nacional de Desarrollo Científico y Tecnológico (FONDECYT, Chile) and Engineering and the Physcial Sciences Research Council (EPSRC, United Kingdom).

Notes

The authors declare no competing financial interest.

ACKNOWLEDGMENTS

F.Q. and J.E. acknowledge financial support from FONDECYT (Chile) under the Postdoctoral Fellowship N° 3140036 and Regular N° 1140132. A.C. acknowledges financial support from EPSRC grant EP/G036780/1. F.Q. would like to thank Mr. Thiago Rossetto Moreschi (Membracel, Brazil) for kindly providing bacterial cellulose pellicles and Dr. Catalina David (Horiba Scientific, France) for her technical assistance in the 2D Raman imaging. Dr. Silvia Matiacevich (USACH, Chile) and Dr. Cristian Acevedo (UFTSM, Chile) are acknowledged for providing access to, respectively, UV-Visible spectrophotometry and scanning electron microscopy.

REFERENCES

(1) Hinterwaldner, R., *The Science and technology of gelatin*. Academic Press: London ; New York, 1977.

(2) Karim, A. A.; Bhat, R. *Trends in Food Science & Technology* **2008,** *19*, 644-656.

(3) Gómez-Guillén, M. C.; Pérez-Mateos, M.; Gómez-Estaca, J.; López-Caballero, E.; Giménez, B.; Montero, P. *Trends in Food Science & Technology* **2009,** *20*, 3-16.

(4) Mahony, O.; Tsigkou, O.; Ionescu, C.; Minelli, C.; Ling, L.; Hanly, R.; Smith, M. E.; Stevens, M. M.; Jones, J. R. *Adv. Funct. Mater.* **2010,** *20*, 3835-3845.

(5) Van Vlierberghe, S.; Dubruel, P.; Schacht, E. *Biomacromolecules* **2011,** *12*, 1387-1408.

(6) Silva-Weiss, A.; Ihl, M.; Sobral, P. J. A.; Gómez-Guillén, M. C.; Bifani, V. *Food Eng. Rev.* **2013,** *5*, 200-216.

(7) Yakimets, I.; Wellner, N.; Smith, A. C.; Wilson, R. H.; Farhat, I.; Mitchell, J. *Polymer* **2005,** *46*, 12577-12585.

(8) Wihodo, M.; Moraru, C. I. *J. Food Eng.* **2013,** *114*, 292-302.

(9) Eichhorn, S. J.; Dufresne, A.; Aranguren, M.; Marcovich, N. E.; Capadona, J. R.; Rowan, S. J.; Weder, C.; Thielemans, W.; Roman, M.; Renneckar, S.; Gindl, W.; Veigel, S.; Keckes, J.; Yano, H.; Abe, K.; Nogi, M.; Nakagaito, A. N.; Mangalam, A.; Simonsen, J.; Benight, A. S.; Bismarck, A.; Berglund, L. A.; Peijs, T. *J. Mater. Sci.* **2010,** *45*, 1-33.

(10) Lee, K.-Y.; Aitomäki, Y.; Berglund, L. A.; Oksman, K.; Bismarck, A. *Compos. Sci. Technol.* **2014,** *105*, 15-27.

(11) Fadel, S. M.; Hassan, M. L.; Oksman, K. *J. Compos. Mater.* **2012,** *47*, 1977-1985.

(12) Chang, S.-T.; Chen, L.-C.; Lin, S.-B.; Chen, H.-H. *Food Hydrocolloids* **2012,** *27*, 137-144.

(13) George, J.; Siddaramaiah. *Carbohydr. Polym.* **2012,** *87*, 2031-2037.

(14) Santos, T. M.; Souza Filho, M. d. S. M.; Caceres, C. A.; Rosa, M. F.; Morais, J. P. S.; Pinto, A. M. B.; Azeredo, H. M. C. *Food Hydrocolloids* **2014,** *41*, 113-118.

(15) Mondragon, G.; Peña-Rodriguez, C.; González, A.; Eceiza, A.; Arbelaiz, A. *Eur. Polym. J.* **2015,** *62*, 1-9.

(16) Klemm, D.; Philipp, B.; Heinze, T.; Heinze, U.; Wagenknecht, W., Introduction. In *Comprehensive Cellulose Chemistry*, Klemm, D., Ed. Wiley-VCH Verlag GmbH & Co. KGaA: 1998; pp 1-7.

(17) Guhados, G.; Wan, W.; Hutter, J. L. *Langmuir* **2005,** *21*, 6642-6646.

(18) Tanpichai, S.; Quero, F.; Nogi, M.; Yano, H.; Young, R. J.; Lindström, T.; Sampson, W. W.; Eichhorn, S. J. *Biomacromolecules* **2012,** *13*, 1340-1349.

(19) Woehl, M. A.; Canestraro, C. D.; Mikowski, A.; Sierakowski, M. R.; Ramos, L. P.; Wypych, F. *Carbohydr. Polym.* **2010,** *80*, 866-873.

(20) Lee, K.-Y.; Blaker, J. J.; Bismarck, A. *Compos. Sci. Technol.* **2009,** *69*, 2724-2733.

(21) Quero, F.; Nogi, M.; Yano, H.; Abdulsalami, K.; Holmes, S. M.; Sakakini, B. H.; Eichhorn, S. J. *ACS Appl. Mater. Interfaces* **2009,** *2*, 321-330.

(22) Gindl, W.; Keckes, J. *Compos. Sci. Technol.* **2004,** *64*, 2407-2413.

(23) Seydibeyoğlu, M. Ö.; Misra, M.; Mohanty, A.; Blaker, J.; Lee, K.-Y.; Bismarck, A.; Kazemizadeh, M. *J. Mater. Sci.* **2013,** *48*, 2167-2175.

(24) Brown, E.; Zhang, J.; Laborie, M.-P. *Cellulose* **2011,** *18*, 631-641.

(25) Schramm, M.; Hestrin, S. *J. Gen. Microbiol.* **1954,** *11*, 123-129.

(26) Díaz-Calderón, P.; Caballero, L.; Melo, F.; Enrione, J. *Food Hydrocolloids* **2014,** *39*, 171-179.

(27) Segal, L.; Creely, J. J.; Martin, A. E.; Conrad, C. M. *Text. Res. J.* **1959,** *29*, 786-794.

(28) Bragg, W. L. *Proc. Camb. Philos. Soc.* **1913,** *17*, 43-57.

(29) Wiley, J. H.; Atalla, R. H. *Carbohydr. Res.* **1987,** *160*, 113-129.

(30) Zhang, L.; Henson, M. J.; Sekulic, S. S. *Anal. Chim. Acta* **2005,** *545*, 262-278.

(31) Marquardt, D. W. *J. Soc. Ind. Appl. Math.* **1963,** *11*, 431-441.

(32) Eichhorn, S. J.; Sirichaisit, J.; Young, R. J. *J. Mater. Sci.* **2001,** *36*, 3129-3135.

(33) Rusli, R.; Eichhorn, S. J. *Appl. Phys. Lett.* **2008,** *93*, 033111.

(34) Šturcová, A.; Davies, G. R.; Eichhorn, S. J. *Biomacromolecules* **2005,** *6*, 1055-1061.

(35) Krenchel, H. *Akademisk Forlag, Copenhagen* **1964**.

(36) Quero, F.; Nogi, M.; Lee, K.-Y.; Poel, G. V.; Bismarck, A.; Mantalaris, A.; Yano, H.; Eichhorn, S. J. *ACS Appl. Mater. Interfaces* **2010,** *3*, 490-499.

(37) Jing, W.; Yizao, W.; Jing, H.; Xinwei, L.; Tao, Y.; Chuan, G. *Micro Nano Lett.* **2011,** *6*, 133-136.

(38) Park, S.; Baker, J.; Himmel, M.; Parilla, P.; Johnson, D. *Biotechnol. Biofuels* **2010,** *3*, 10.

(39) French, A. *Cellulose* **2014,** *21*, 885-896.

(40) Badii, F.; MacNaughtan, W.; Mitchell, J. R.; Farhat, I. A. *Drying Technol.* **2013,** *32*, 30-38.

(41) Bigi, A.; Panzavolta, S.; Rubini, K. *Biomaterials* **2004,** *25*, 5675-5680.

(42) Althues, H.; Henle, J.; Kaskel, S. *Chem. Soc. Rev.* **2007,** *36*, 1454-1465.

(43) Beecroft, L. L.; Ober, C. K. *Chemistry of Materials* **1997,** *9*, 1302-1317.

(44) Nogi, M.; Yano, H. *Advanced Materials* **2008,** *20*, 1849-1852.

(45) Seeboth, A.; Hermel, H. *Thin Solid Films* **1989,** *173*, L119-L121.

(46) Bjelkhagen, H. I., *Silver-Halide Recording Materials for Holography and Their Processing*. 2nd ed.; 1993; Vol. 66, p 441.

(47) Maneerat, C.; Hayata, Y.; Muto, N.; Kuroyanagi, M. *J. Food Prot.* **2003,** *66*, 2168-2170.

(48) Ordidge, M.; García-Macías, P.; Battey, N. H.; Gordon, M. H.; John, P.; Lovegrove, J. A.; Vysini, E.; Wagstaffe, A.; Hadley, P. *J. Sci. Food Agric.* **2012,** *92*, 1597-1604.

(49) Gierlinger, N.; Schwanninger, M.; Reinecke, A.; Burgert, I. *Biomacromolecules* **2006,** *7*, 2077-2081.

(50) Rusli, R.; Shanmuganathan, K.; Rowan, S. J.; Weder, C.; Eichhorn, S. J. *Biomacromolecules* **2010,** *11*, 762-768.

(51) Quero, F.; Eichhorn, S.; Nogi, M.; Yano, H.; Lee, K.-Y.; Bismarck, A. *J. Polym. Environ.* **2012,** *20*, 916-925.

(52) Tanpichai, S.; Sampson, W. W.; Eichhorn, S. J. *Composites, Part A* **2012,** *43*, 1145-1152.

(53) Tanpichai, S.; Sampson, W. W.; Eichhorn, S. J. *Composites, Part A* **2014,** *65*, 186-191.

(54) Bulota, M.; Tanpichai, S.; Hughes, M.; Eichhorn, S. J. *ACS Appl. Mater. Interfaces* **2012,** *4*, 331-337.

Table of Contents Use Only

Manuscript title: Stress Transfer Quantification in Gelatin-Matrix Composites with Tunable Optical Properties

Authors: Franck Quero, Abigail Coveney, Anna E. Lewandowska, Robert Richardson, Paulo Díaz-Calderón, Koon-Yang Lee, Stephen J. Eichhorn, Ashraf Alam, Javier Enrione

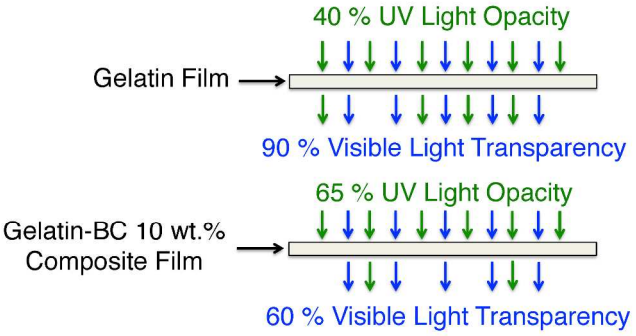

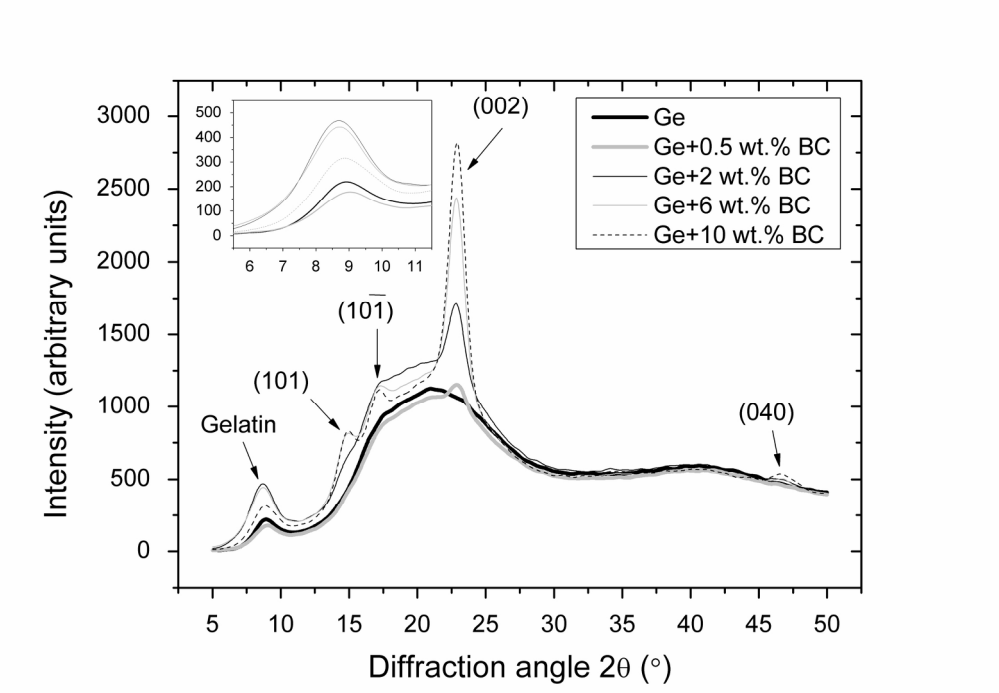

Figure 1. Typical X-ray diffraction patterns for gelatin and gelatin-bacterial cellulose (BC) composites at various weight fractions (wt.%). The inset represent the diffraction peak located at approximately 2θ = 9°, corresponding to the triple helix configuration of gelatin.
192x135mm (300 x 300 DPI)

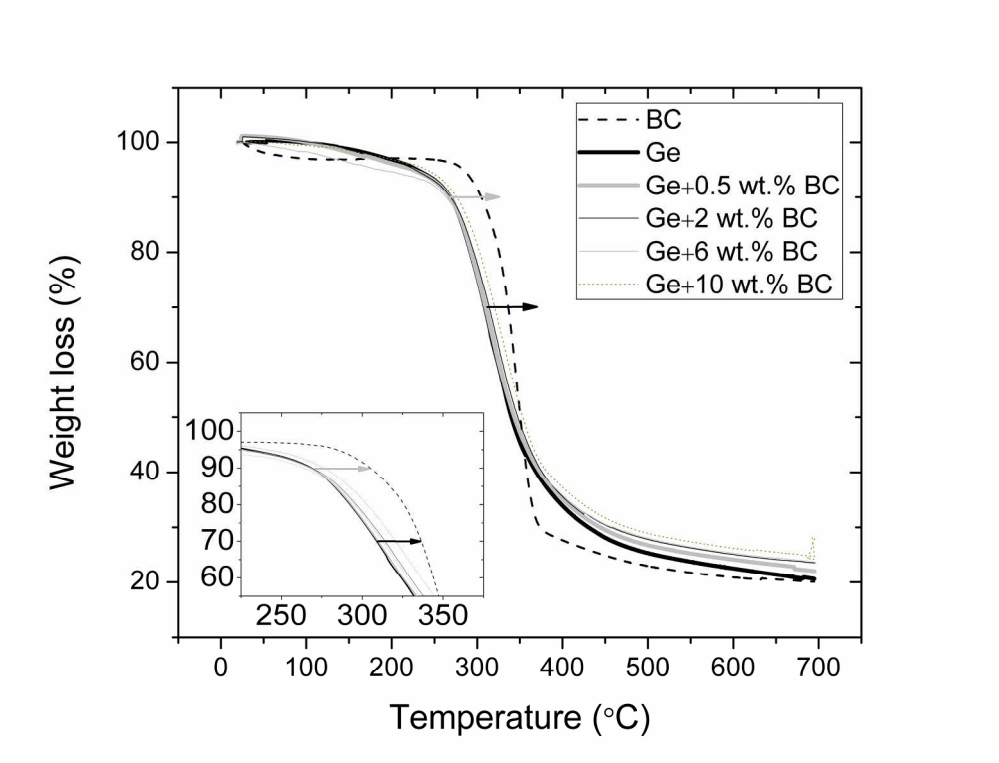

Figure 2. Typical thermograms for BC, gelatin and gelatin-BC composites. The arrows indicate the shift of the onset (grey) and peak (black) degradation temperature upon addition of BC to the gelatin matrix. The inset represents the same thermograms from 225 to 375 °C.
208x159mm (300 x 300 DPI)

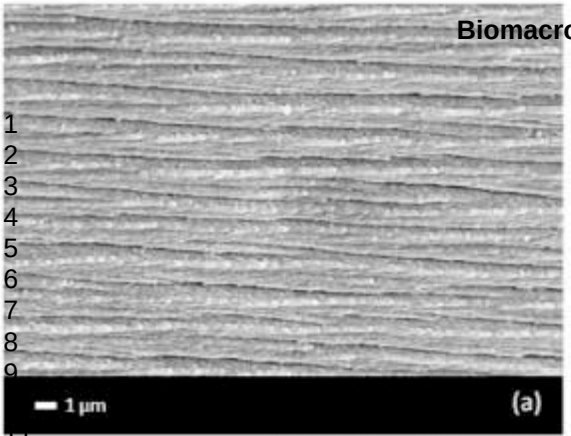

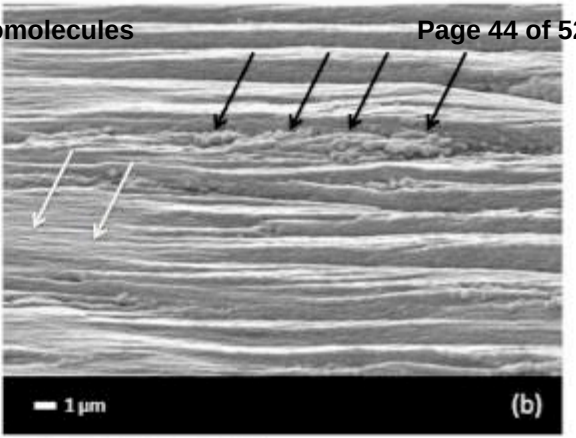

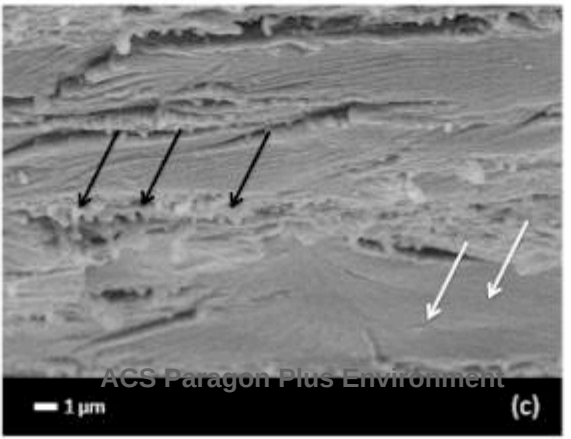

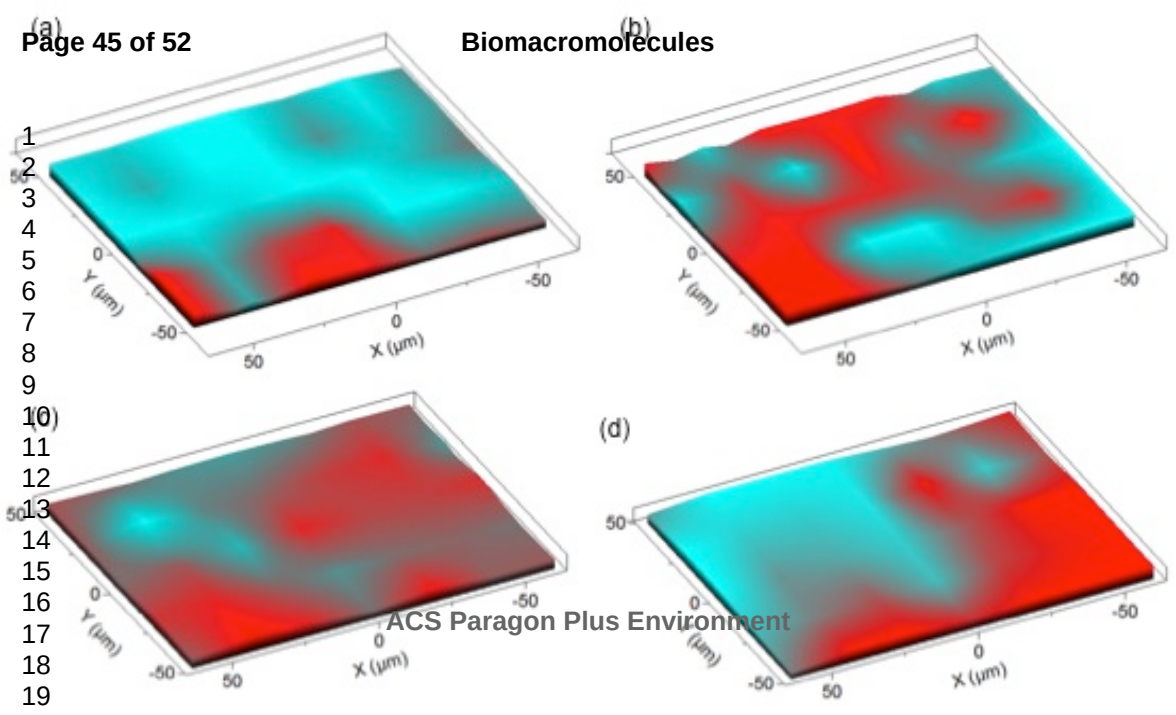

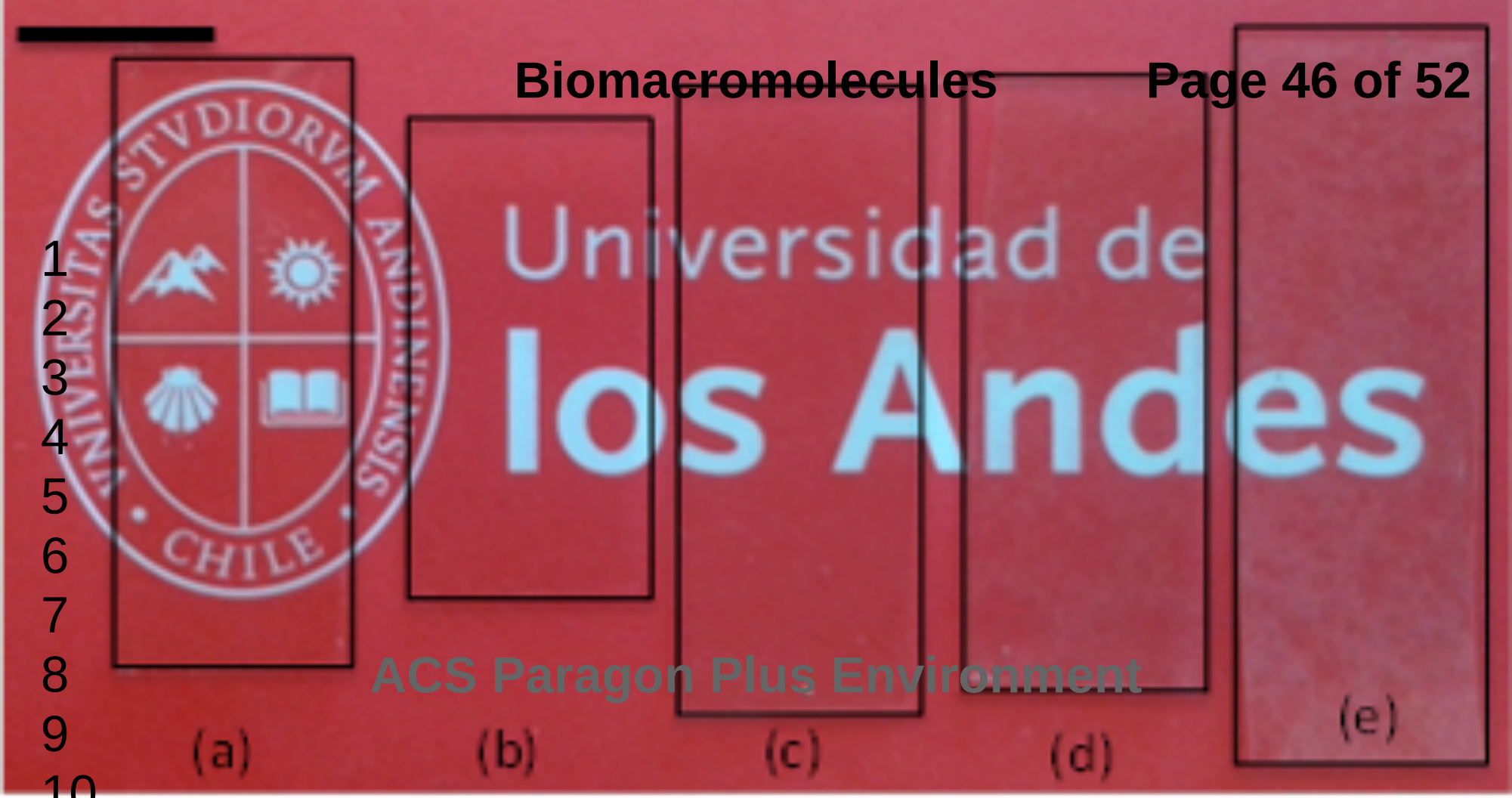

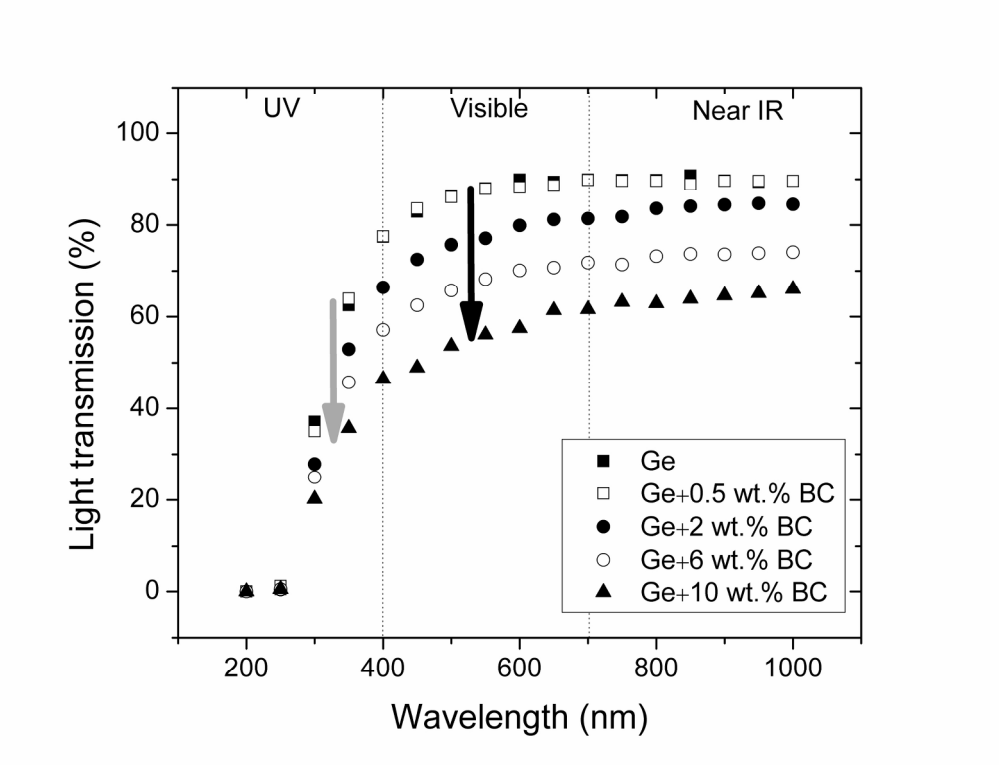

Figure 6. Transmittance spectra of gelatin (Ge) and Ge-bacterial cellulose (BC) composites with BC loadings 0.5, 2, 6 and 10 wt.%. The black and grey arrows indicate a reduction in transparency to visible and UV wavelengths, respectively.
208x159mm (300 x 300 DPI)

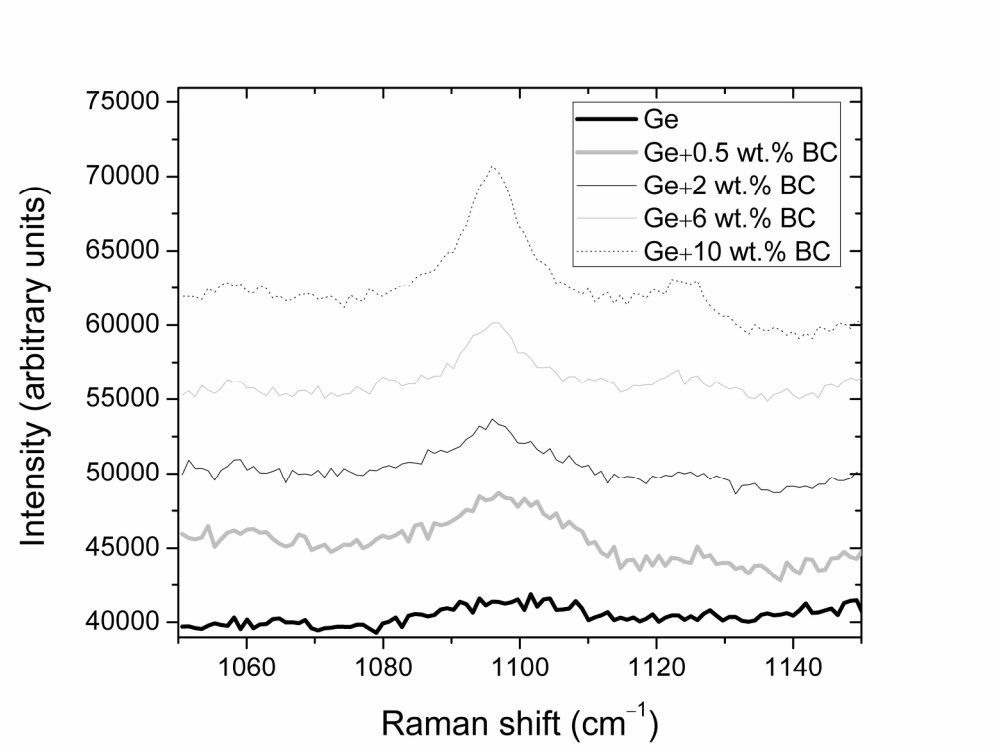

Figure 7. Typical Raman spectra for gelatin and gelatin-BC composite films (0.5, 2, 6 and 10 wt.%) in the Raman shift range of 1050 to 1150 cm-1.
208x159mm (300 x 300 DPI)

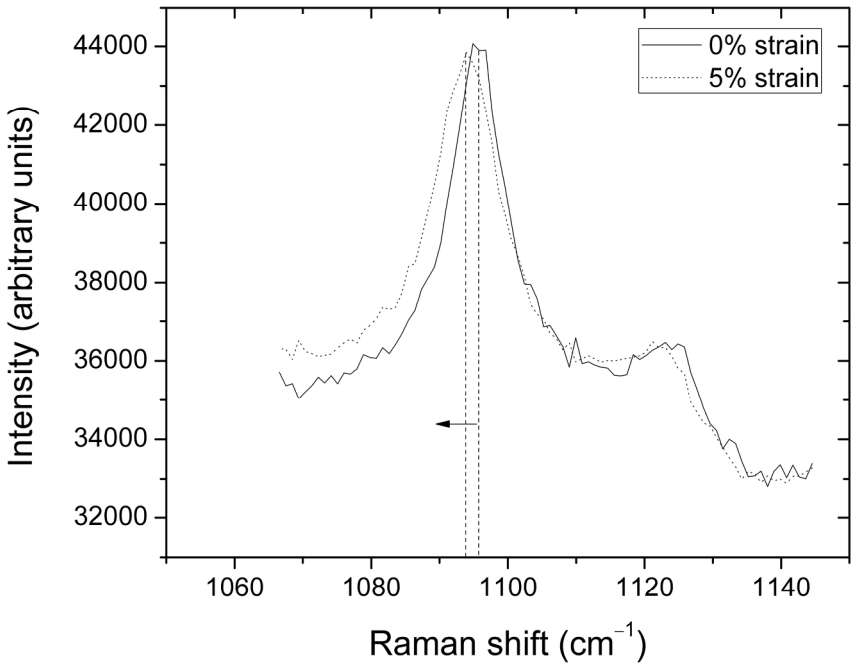

Figure 8. Typical shift towards a lower wavenumber position of the Raman band corresponding to vibrational modes of C-O and C-O-C moieties in the cellulose backbone upon application of external tensile deformation. Arrow indicates the direction of the band shift towards a lower wavenumber with increasing strain. Data shown are for a 10 wt.% gelatin-BC composite film.
208x159mm (300 x 300 DPI)

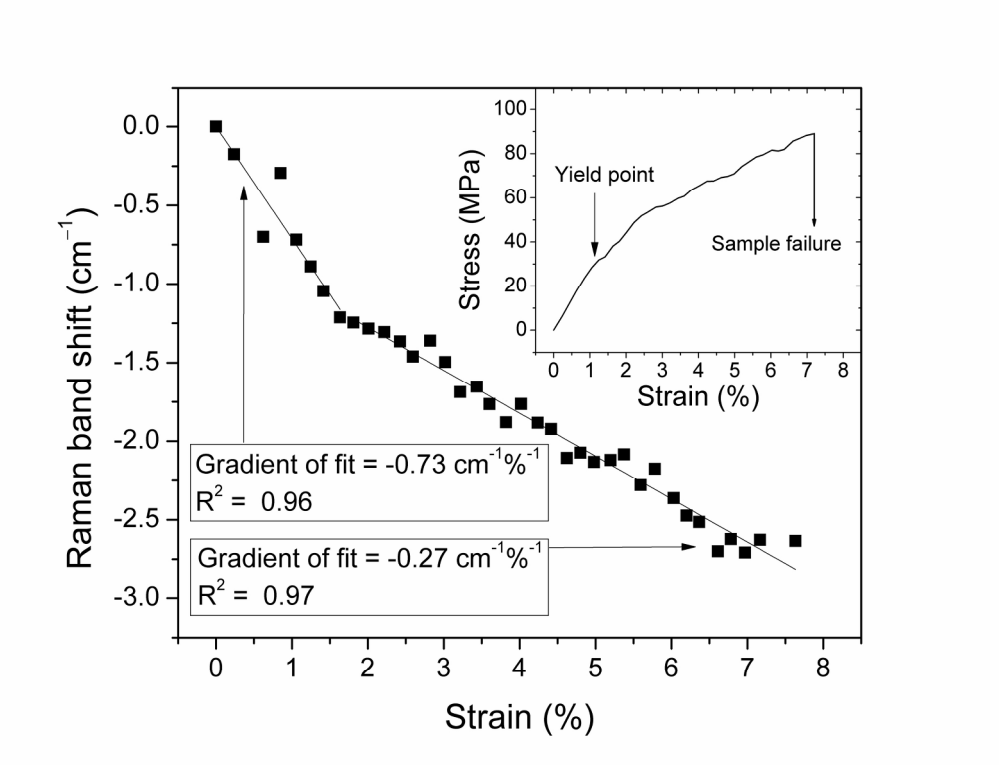

Figure 9. Typical shifts in the position of the Raman band corresponding to vibrational modes of C-O and C-O-C moieties in the backbone of cellulose as a function of strain. Results are shown for a 10 wt.% gelatin-BC composite film. The inset represents a typical stress-strain curve obtained for the same material. Solid lines are linear fits to the data.
208x159mm (300 x 300 DPI)

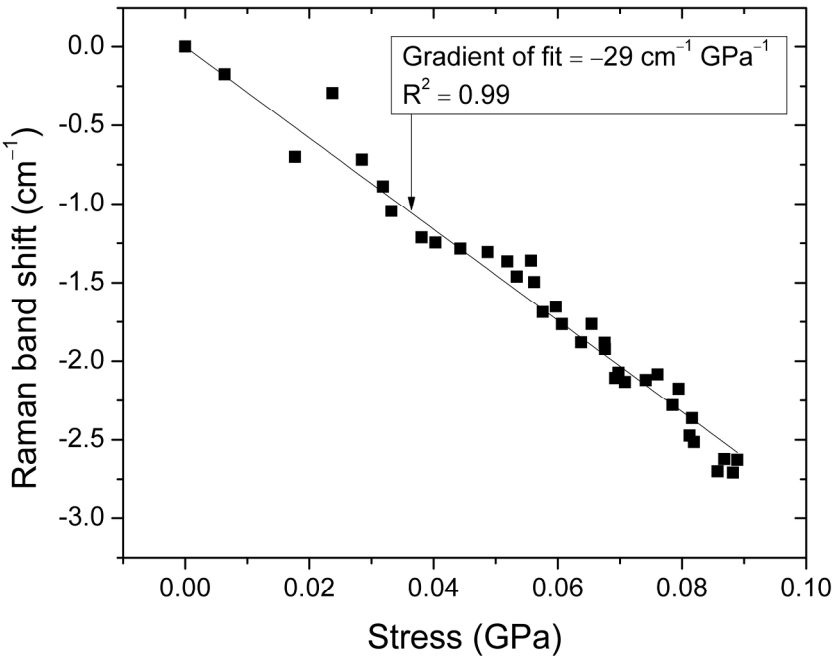

Figure 10. Typical shifts in the position of the Raman band corresponding to vibrational modes of C-O and C-O-C moieties in the backbone of cellulose as a function of stress. Results shown are for a 10 wt.% gelatin-BC composite film.
208x159mm (300 x 300 DPI)

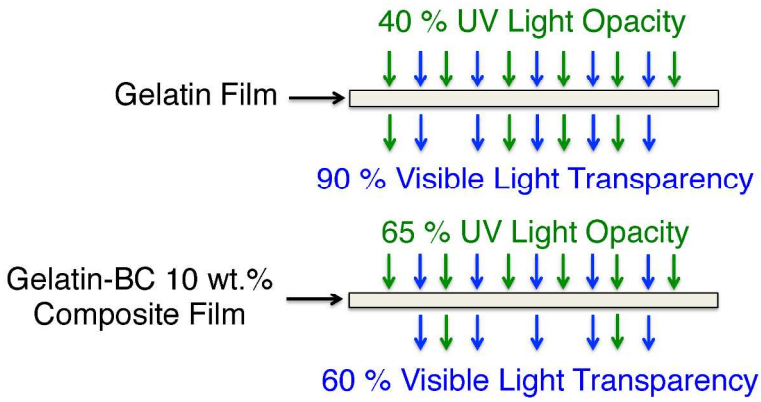

254x190mm (300 x 300 DPI)